

Laser-Cooling-Assisted Mass Spectrometry

Christian Schneider,* Steven J. Schowalter, Kuang Chen, Scott T. Sullivan, and Eric R. Hudson

Department of Physics and Astronomy, University of California, Los Angeles, California 90095, USA

(Received 15 April 2014; published 30 September 2014)

Mass spectrometry is used in a wide range of scientific disciplines including proteomics, pharmaceuticals, forensics, and fundamental physics and chemistry. Given this ubiquity, there is a worldwide effort to improve the efficiency and resolution of mass spectrometers. However, the performance of all techniques is ultimately limited by the initial phase-space distribution of the molecules being analyzed. Here, we dramatically reduce the width of this initial phase-space distribution by sympathetically cooling the input molecules with laser-cooled, cotrapped atomic ions, improving both the mass resolution and detection efficiency of a time-of-flight mass spectrometer by over an order of magnitude. Detailed molecular-dynamics simulations verify the technique and aid with evaluating its effectiveness. This technique appears to be applicable to other types of mass spectrometers.

DOI: 10.1103/PhysRevApplied.2.034013

I. INTRODUCTION

Mass spectrometry (MS) is an integral tool in modern science, constituting a roughly \$4 billion annual market [1,2]. It is used to identify assays in hospitals and forensics laboratories [3,4], characterize complex proteins [5], discover and produce pharmaceuticals [6], and enable important measurements in fundamental physics and chemistry [7]. Given this ubiquity, there is a worldwide effort to develop mass spectrometers with ever-improving performance [8–12].

The performance of a mass spectrometer is primarily characterized by two numbers: the mass resolution, calculated as $m/\Delta m$, where m is the mass of the molecule being analyzed and Δm is the imprecision of the mass measurement, and the detection limit, which is the minimum number of molecules required to produce a useful signal in the spectrometer. Fundamentally, a mass spectrometer operates by separating the initial phase-space volume of the molecules under study, i.e., the assay, into distinct phase-space volumes in a mass-dependent way. For example, in a time-of-flight mass spectrometer (TOFMS) mass-dependent propagation delays are used to separate the initial phase-space volume, while in a Fourier-transform mass spectrometer the mass dependence of an orbital frequency is used. In an ideal mass spectrometer, each mass in the assay would be mapped to a single point in phase space, allowing infinite mass resolution and detection of every molecule in the assay.

Unfortunately, the separation techniques employed in mass spectrometers are generally dissipationless, and, thus, according to Liouville's theorem, the phase-space volume cannot be compressed. Therefore, the ideal mass-spectrometer performance can be realized only if the molecular phase-space distribution begins with zero width.

However, practical considerations for a mass spectrometer are at odds with this desire for a small initial phase-space volume. Because of the relative ease of manipulating and detecting charged particles, modern mass spectrometers analyze molecules that have been vaporized and ionized. These ions are typically produced by using techniques, such as electrospray ionization [13,14] and matrix-assisted laser desorption/ionization [15–17], which create ionized assays of input molecules with large kinetic energy, several $k_B \times (10^3\text{--}10^5)$ K. To combat the large width of the phase-space distribution that comes with these elevated temperatures and improve performance, commercial mass spectrometers typically employ a collisional-cooling stage [12,18–23] with an inert, room-temperature buffer gas, as originally demonstrated for guided ions in Ref. [24]. This cooling narrows the input phase space distribution and improves, to an extent, mass spectrometer performance.

To further mitigate the effects of the initial phase-space distribution, several techniques [8–12] have been developed, which effectively squeeze the phase-space volume in one dimension and/or make the mass spectrometer insensitive to a spread in a certain dimension. Nonetheless, improved mass resolution using these techniques often comes at the price of a reduced detection efficiency (or vice versa), because practical limitations, such as machining imprecisions, ultimately limit their efficiency. Furthermore, some techniques intentionally restrict mass analysis to only a fraction of the available phase-space distribution for increased resolution.

Here, we propose and demonstrate a method, called laser-cooling-assisted mass spectrometry (LAMS), to dramatically reduce the width of the molecular phase-space distribution by cooling the assay to temperatures up to 6 orders of magnitude lower than traditional room-temperature buffer-gas cooling. Input molecules are sympathetically cooled [25,26] with laser-cooled,

*christian.schneider@physics.ucla.edu

cotrapped atomic ions prior to mass analysis (hereafter referred to as LAMS[X^+], where X^+ denotes the laser-cooled species). The spread of the phase-space distribution in momentum space is virtually eliminated, while the extent of the spatial component of the distribution is limited only by the balance of the confining potential holding the assay and the Coulomb repulsion between constituent ions. By implementing LAMS in a traditional TOFMS, we demonstrate an improvement in both mass resolution and detection limit of over an order of magnitude. Sympathetic cooling has previously been suggested to improve the mass spectrometry of highly charged ions in a Penning trap by extending trap lifetimes and enabling longer interrogation times [27–29]. Additionally, sympathetic cooling has shown improvement of mass resolution in the extraction method with rf traps [30,31].

Although LAMS is demonstrated with a TOFMS, this technique appears to be applicable to other types of mass spectrometers. In its current form, the technique can be used to assay compounds up to a mass of approximately 10^3 Da, which includes volatile organic compounds, the amino acids, explosive agents, and some peptides; modifications may extend the technique to include heavier biomolecules such as nucleic acids.

In the remainder of this article, we report on the results of a proof-of-principle experiment using LAMS with a basic, Wiley-McLaren-type TOFMS [8]. Our TOFMS does not utilize a reflectron [10] or other advanced engineering techniques, so that the effectiveness of LAMS can be judged independently of these techniques. Along with a discussion of the improvements in mass resolution, detailed molecular-dynamics simulations are presented, which reproduce our experimental findings and aid evaluation of the effectiveness of LAMS. We conclude with possible uses and future steps to be taken using this powerful method.

II. EXPERIMENTAL SETUP

The apparatus consists of a segmented linear quadrupole trap (LQT), and a basic, Wiley-McLaren-type TOFMS (see Fig. 1 for a schematic, similar to the apparatus previously outlined in Ref. [32]). The LQT has a field radius of $R_0 = 6.85$ mm and is driven asymmetrically (two diagonally opposing electrodes at rf voltage V_0 , and the others at rf ground) at a frequency of $\Omega \approx 2\pi \times 0.7$ MHz and an rf amplitude of $V_0 = 250$ V. Samples of atoms and molecules are loaded into the LQT by ablating a metallic Yb target or a pressed, annealed BaCl_2 target with a pulsed Nd:YAG laser. The assays are exposed to laser beams to Doppler cool a single isotope of either Ba^+ or Yb^+ . These laser beams are roughly aligned along the axis of the LQT and retroreflected at the exit viewport. For Ba^+ (Yb^+), a Doppler cooling beam at 493 nm (369 nm) and a repump beam at 650 nm (935 nm) are required. In the case of Ba^+ , a magnetic field is applied to destabilize dark states, which result from the Λ system [33]. Because of their Coulomb

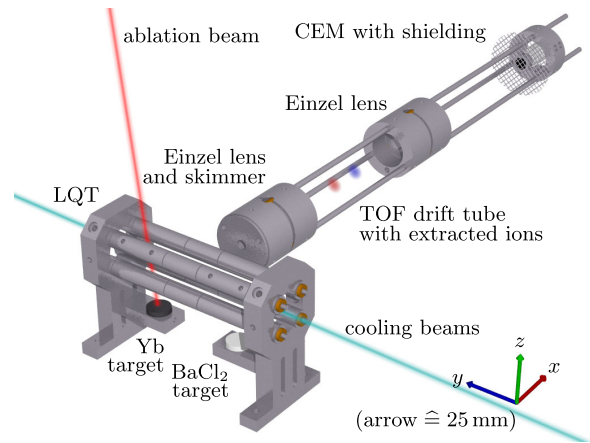


FIG. 1. Schematic of the LAMS apparatus. The LQT has a field radius of $R_0 = 6.85$ mm and a length of 91 mm. Its axis is aligned perpendicularly to the TOF drift tube to enable the radial extraction. The Yb and BaCl_2 ablation targets are mounted below the LQT. The laser-cooling beams are roughly aligned with the axis of the LQT. The TOF drift tube contains two Einzel lenses and has a total length of 275 mm. Ions are detected by using a channel electron multiplier (CEM), which is shielded by a grounded stainless-steel mesh, and the complete assembly is held under vacuum at a pressure of approximately 10^{-9} mbar. The fluorescence of the laser-cooled species is imaged through an objective lens (not shown), facing the TOFMS, onto an electron-multiplying CCD camera and allows estimation of the number of atoms and molecules in the assay.

interaction with the laser-cooled species, other atoms and molecules in the trap are sympathetically cooled, and the full assay reaches temperatures of (1–100) mK.

Subsequently, the rf voltage is turned off within a fraction of an rf cycle, and the electrodes are pulsed to dc high voltages (HV) with a 10%–90% rise time of approximately 250 ns. The HV is applied such that a two-stage electric field is established [8], which radially extracts the cold atoms and molecules from the LQT into the TOFMS [34,35]. This extraction is accomplished by applying a slightly lower HV to the electrodes which are closer to the TOFMS (1.2 kV) than to the ones that are farther (1.4 kV). The TOF drift tube has a length of 275 mm, and its entrance is determined by a grounded skimmer with an aperture diameter of 5.6 mm. It contains two Einzel lenses which allow the focusing of the molecules. For the experiments presented here, a voltage of approximately 900 V (approximately 500 V) is applied to the front (rear) Einzel lens. The molecules are detected with a CEM, which is shielded from the drift tube by a grounded stainless-steel mesh.

III. RESULTS

To precisely measure the attainable mass resolution, metallic Yb, having seven naturally abundant isotopes, is assayed in this demonstration of LAMS. The Yb target is ablated and $^{174}\text{Yb}^+$ ions are laser cooled

(LAMS $^{[174}\text{Yb}^+]$). The average assay size is approximately 1000 ions. Once laser cooled, we extract the assay into the TOF drift tube and record the TOF spectrum. The average of 20 spectra for the LAMS $^{[174}\text{Yb}^+]$ experiment is depicted in Fig. 2 (blue curve) and compared to the spectrum of the traditional TOFMS without laser cooling (red curve). As the flight time T and mass m of a molecule are connected through $T \propto \sqrt{m}$, we use the dominant signal of $^{174}\text{Yb}^+$ corresponding to a flight time of $T_{174} \approx 9.84 \mu\text{s}$ and mass $m_{174} = 173.94 \text{ Da}$ for mass calibration [36].

The peaks in the LAMS $^{[174}\text{Yb}^+]$ spectrum have a full width at half maximum of $\Delta m_{\text{LAMS}} \approx 0.35 \text{ Da}$. This result corresponds to a mass resolution of $m/\Delta m \approx 500$ and allows isotopic resolution. All peaks can be explained by the naturally abundant isotopes of ytterbium: ^{168}Yb (< 1%), ^{170}Yb (3%), ^{171}Yb (14%), ^{172}Yb (22%), ^{173}Yb (16%), ^{174}Yb (32%), and ^{176}Yb (13%) [37]. The peak in the traditional TOFMS spectrum is a superposition of peaks belonging to these Yb^+ isotopes. Hence, its width of approximately 7 Da does not directly reflect the mass resolution of the traditional TOFMS but corresponds to a single-isotope width of $\Delta m_{\text{TOFMS}} \approx 5 \text{ Da}$ and mass resolution of $m/\Delta m_{\text{TOFMS}} \approx 35$. Compared to the traditional TOFMS, LAMS constitutes an improvement in mass resolution of more than an order of magnitude. Though the recorded signal intensities are also enhanced by more than an order of magnitude over traditional TOFMS, the LAMS signals are so large that they lead to partial saturation of the CEM. Thus, it is difficult to measure the true gain in detection sensitivity; however, simulation suggests an improvement for LAMS of approximately 30 times over traditional TOFMS with 300-K assays. Saturation of the detector also explains the broadening

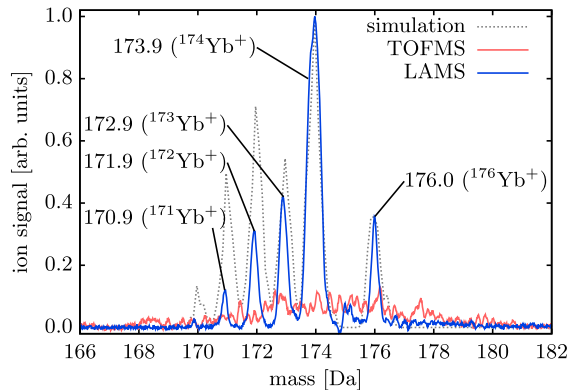


FIG. 2. LAMS $^{[174}\text{Yb}^+]$ versus traditional TOFMS for trapped Yb ablation products. Samples consisting of approximately 1000 ions are loaded into the LQT, and $^{174}\text{Yb}^+$ is laser cooled. The LAMS curve represents the average of 20 spectra. The labels denote the mass of the ions of the corresponding peak and are determined by a fit of a Gaussian curve to the LAMS spectrum. For comparison, a traditional TOFMS curve, which is an average of 20 spectra taken without laser cooling, and a simulation of a LAMS spectrum (see the text) are shown.

of the $^{174}\text{Yb}^+$ peak ($\Delta m_{174} \approx 0.5 \text{ Da}$) and prevents reliable estimates of the abundances of different molecules in our assay; according to fluorescence images, we expect a higher abundance of $^{174}\text{Yb}^+$ than the peak heights suggest. As there is no naturally abundant ^{175}Yb , the small peak at $m \approx 175 \text{ Da}$ could be due to the presence of $^{174}\text{Yb}^1\text{H}^+$ in our assays or an electronics artifact resulting from the large, preceding signal, which is supported by the additional, slight undershooting before this peak.

Figure 2 also shows the result of a molecular-dynamics simulation [38] of LAMS $^{[174}\text{Yb}^+]$. For this simulation, the electric field of the LQT is solved by using a boundary-element method [39]. The simulation includes micromotion of the ions trapped in the LQT, mutual ion-ion Coulomb interaction, and the experimental, time-dependent voltages applied to the electrodes of the LQT. For each simulated spectrum, the initial conditions of the ions are generated in a Monte Carlo fashion followed by applying a fictitious damping force. The resulting ion cloud has a temperature $T \sim 0.25 \text{ K}$ for the secular ion motion and does not form an ion Coulomb crystal. The curve is the average of 20 simulated spectra with an assay size of approximately 500 Yb^+ ions with natural isotopic abundances. As the Einzel lenses are not included in the simulation and the experimental voltages are known only within 3%, the simulated flight times show a deviation by approximately $0.5 \mu\text{s}$ from the flight times observed in the experiment. Hence, we perform a separate mass calibration for the simulated data. The simulation agrees well with the experimental results and predicts a detection efficiency of 50%. However, as the Einzel lenses are not considered in the simulation, this result is likely a lower bound on the detection efficiency. For larger assays, this number goes down slightly due to the axially elongated assay being clipped by both the skimmer and the aperture of the CEM.

In the second LAMS demonstration, we analyze the ablation products of BaCl_2 to demonstrate the effectiveness of LAMS for sympathetically cooled constituents of an assay over a broader mass range. Here, we laser cool $^{138}\text{Ba}^+$ (LAMS $^{[138}\text{Ba}^+]$) and use an assay size of approximately 1000 ions. The average of 20 spectra for the LAMS $^{[138}\text{Ba}^+]$ is shown in Fig. 3 (blue curve) and again compared to the traditional TOFMS spectrum without any laser cooling (red curve). The $^{138}\text{Ba}^+$ peak is used for mass calibration ($m_{138} = 137.9 \text{ Da}$) and leads to the same calibration as for the (experimental) LAMS $^{[174}\text{Yb}^+]$ spectrum.

The peaks in the LAMS $^{[138}\text{Ba}^+]$ spectrum at $m = 172.9 \text{ Da}$ and $m = 174.9 \text{ Da}$ can be explained by the presence of $^{138}\text{Ba}^{35}\text{Cl}^+$ and $^{138}\text{Ba}^{37}\text{Cl}^+$, respectively. The natural abundance of ^{138}Ba amounts to 72% (other Ba isotopes are lighter and have at most 11% natural abundance [37]), and chlorine naturally consists of ^{35}Cl (76%) and ^{37}Cl (24%). Hence, these BaCl^+ molecules represent by far the most abundant isotopic pairings, and the signal intensities qualitatively match the natural

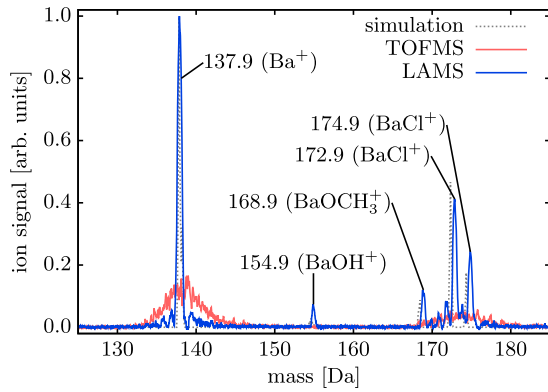


FIG. 3. LAMS[$^{138}\text{Ba}^+$] versus traditional TOFMS for trapped BaCl_2 ablation products. Compared to Fig. 2, slightly larger assays are used for the LAMS (of the order of few thousand ions) and $^{138}\text{Ba}^+$ is laser cooled. The LAMS curve represents the average of 20 spectra. The labels denote the mass of the ions of the corresponding peak and are determined by a fit of a Gaussian curve to the LAMS spectrum. For comparison, a traditional TOFMS curve, which is an average of 20 spectra taken without laser cooling, and a simulation of a LAMS spectrum (see the text) are shown.

abundances of the respective isotopes. The peak at $m = 154.9$ Da most likely represents $^{138}\text{Ba}^{16}\text{O}^1\text{H}$; see Ref. [32]. The peak at $m = 168.9$ Da appears to be due to $^{138}\text{Ba}^{16}\text{O}^{12}\text{C}^1\text{H}_3^+$, a reaction product of barium and methanol, as methanol was used in the preparation of the BaCl_2 target. Additionally, the LAMS[$^{138}\text{Ba}^+$] spectrum reveals the presence of the lighter Ba^+ isotopes next to the $^{138}\text{Ba}^+$, $^{138}\text{Ba}^{35}\text{Cl}^+$, and $^{138}\text{Ba}^{37}\text{Cl}^+$ peaks. The peaks at $m \approx 139$ Da and $m \approx 176$ Da are, as already observed in the LAMS[$^{174}\text{Yb}^+$] spectrum, either electronics artifacts or hydride ions.

The simulation of LAMS[$^{138}\text{Ba}^+$] is performed analogously to the simulation of LAMS[$^{174}\text{Yb}^+$]. Each individual simulation considers a total of approximately 500 ions comprising the above-mentioned molecules, and the curve in Fig. 3 is an average of 20 such simulated spectra. The deviation between experimental data and simulation is slightly larger than for LAMS[$^{174}\text{Yb}^+$]. Presumably, this difference can be explained due to the time-dependent acceleration during the turn-on of the extraction high voltages, which can result in a (slight) departure of the mass calibration from the ideal $T \propto \sqrt{m}$ relation. As we know the extraction voltages only within 3%, the magnitude of the observed deviation is not surprising.

For the data of Fig. 2 and 3, Einzel lenses are used to focus molecules with trajectories deviating from the axis of the drift tube onto the CEM, increasing the detection efficiency. These trajectories are longer than those of the on-axis molecules, leading to a broadening in the mass spectrum in traditional TOFMS [32]. However, when using LAMS, we have observed that, while the use of the Einzel lenses does improve the detection efficiency, it does not

noticeably affect the mass resolution. Presumably, this observation is a result of the localization and cooling of the molecules before injection into the TOFMS.

IV. DISCUSSION

The observed improvement in mass resolution with cooling can be easily quantified with a simplified model assuming an ideal Wiley-McLaren TOFMS and using the experimental parameters of the LAMS[Yb^+] experiment, as shown in Fig. 4. Here, only the projection of the position and velocity onto the direction of extraction is considered. The mass resolution is deduced from the difference of the flight times of two ions with opposing initial conditions $(x, v) = \pm(\Delta x, \Delta v)$. Here, Δx and Δv represent twice the standard deviation of Gaussian distributions in x and v , respectively, such that Δx can be interpreted as the radius of the ion cloud and the two ions considered in the calculation correspond roughly to the outmost ions. The repulsion due to $N \sim 1000$ ions of the whole cloud in the LAMS[Yb^+] experiment is simplified as the force exerted by a uniform charge distribution enclosed in a sphere between the two outmost ions. As the rf trap potential in the experiment leads to ion clouds with an radial-to-axial aspect ratio of 1:4, only a total charge of $N/4$ ions is included in this uniform charge distribution. The ions are propagated through the two (ideal) acceleration stages and the drift tube of the TOFMS, and the mass resolution of the TOFMS is derived from their arrival times in the detector plane.

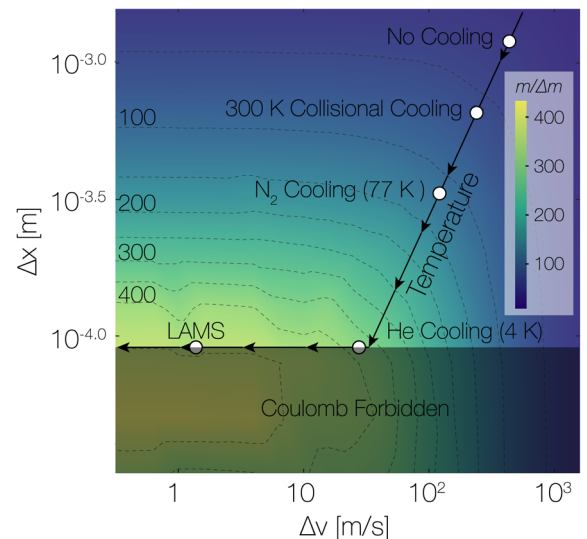


FIG. 4. Mass resolution of an ideal Wiley-McLaren TOF [8] as a function of the width of the velocity (Δv) and spatial distribution (Δx) of the input assay. The simulation assumes an input assay consisting of 1000 $^{174}\text{Yb}^+$ ions and LQT parameters as used in Fig. 2. The ion-ion Coulomb repulsion prohibits further squeezing of the assay's spatial distribution at increasingly lower temperatures (Coulomb-forbidden region). Points correspond to distributions belonging to different cooling methods.

As expected, the mass resolution increases for both a decrease of the width of the velocity Δv and spatial distribution Δx , until the latter is limited by ion-ion repulsion within the trapping potential of the LQT (labeled Coulomb forbidden). Because of ion-ion repulsion, overconfinement ($\Delta x \lesssim 100 \mu\text{m}$ or an ion density of approximately 10^8 cm^{-3}) can even lead to a slight decrease of mass resolution as the large amount of potential energy between the ions is released during extraction. However, for the employed rf trap parameters, this overconfinement regime cannot be reached, because it lies in the Coulomb-forbidden region. Points on this graph in the Δx - Δv plane represent thermal distributions belonging to different cooling methods employed in mass spectrometry. This simple calculation agrees with the observed mass resolution for the traditional TOFMS, buffer-gas cooling from previous studies using the TOFMS in Ref. [32], and LAMS.

The mass range over which LAMS is effective is set by the mass dependence of the ion trap pondermotive potential and the dynamics of the ion-ion sympathetic cooling in this potential. The pondermotive potential depends on the particles' charge-to-mass ratio, leading to a practical limitation to the heaviest, singly charged molecule that can be trapped and analyzed. In our experiment with Yb^+ , we verify that the trap depth can be changed within a factor of approximately 10. Therefore, we expect [40] LAMS[Yb^+] to be effective for singly charged ions with masses up to 10^3 Da. The lightest molecule that can be assayed is set by the dynamics of the ion-ion sympathetic cooling. Because of micromotion interruption, it is increasingly difficult to sympathetically cool an ion, as its mass becomes smaller than the laser-cooled ion [41,42]. Therefore, the mass range for LAMS is limited between masses similar to the coolant ion—as low as 2 Da for LAMS[Be^+] [43]—up to approximately 10^3 Da for singly charged ions. This range includes volatile organic compounds, the amino acids, explosive agents, and some peptides; modifications may extend the mass range to include heavier biomolecules such as nucleic acids [40,44]. Sympathetic cooling of multiply charged proteins with mass approximately 12 390 Da and charge $(12\text{--}17)e$ has been demonstrated in an rf trap in Ref. [31]. By allowing multiply charged ions and slight modifications of the setup, ions with significantly larger masses should be accessible with LAMS.

While the current TOFMS implementation is basic and the mass resolution does not, by far, reach the resolution of state-of-the-art mass spectrometers (for example, $>100\,000$ for the Orbitrap [23]), LAMS appears to be applicable to these mass spectrometers, where it could lead to an even higher mass resolution and/or improved detection limit. However, further work is necessary as phenomena like collective oscillations [45] in Fourier-transform mass spectrometry may preclude some types of mass spectrometers from realizing the full benefits of

LAMS. We emphasize that for LAMS to be effective it is not necessary to cool the assay close to the Doppler cooling limit nor produce ion Coulomb crystals [46]. Even laser detunings of several natural linewidths Γ (e.g., $\Gamma_{\text{Yb}} \approx 2\pi \times 20 \text{ MHz}$ for Yb^+) from the optimal detuning for Doppler cooling do not affect the mass resolution of LAMS, suggesting that LAMS could be easy to implement in commercial mass spectrometers, especially, in comparison to cryogenic cooling.

In the presented form, LAMS represents an easy-to-implement detection method in cold ion experiments that can be used complementarily to (and, perhaps, more robustly than) techniques based on analyzing fluorescence images [40,47–50] or mass spectrometry based on resonant excitation of the secular ion motion [26,30,51]. It is an ideal tool for spectroscopy of molecular ions and significantly outperforms previous implementations [52–55]. LAMS also promises to be an ideal tool for the rapidly emerging field of hybrid atom-ion interactions [56–58]. It allows for large optical access required for these experiments while providing isotopic identification of every trapped atomic or molecular ion. The current implementation of LAMS will be used in ongoing studies of cold reactions of ionic atoms and molecules with neutral atoms [59–61], where it enables the distinction between different reaction products, and efforts towards cooling molecular ions in a hybrid atom-ion trap [62].

In summary, we have demonstrated a method, LAMS, to prepare assays of molecules for mass spectrometry, which outperforms conventional buffer-gas cooling. LAMS improves the mass resolution of a single TOFMS with a comparatively short drift tube of 275 mm from $m/\Delta m \approx 35$ to $m/\Delta m = 500$ and enables isotopic resolution. LAMS also increases the detection efficiency of the mass spectrometer by over an order of magnitude. Saturation effects of the CEM and its comparatively small aperture set the detection limit in our current setup. By using a microchannel plate detector with a larger active area, simulations suggest it is possible to detect every input ion with isotopic resolution.

ACKNOWLEDGMENTS

We thank Peter Yu for assistance in the development of the LQT and TOFMS electronics and John Bollinger for guiding discussions. This work was supported by ARO Award No. W911NF-10-1-0505, NSF Grant No. PHY-1005453, and ARO Award No. W911NF-14-1-0378.

-
- [1] J. R. Yates III, A century of mass spectrometry: From atoms to proteomes, *Nat. Methods* **8**, 633 (2011).
 - [2] *Mass Spectrometry: Limitless Innovation in Analytical Science. Market Forecast: 2013–2017 (table of contents)* (Strategic Directions International, Inc., 2012).

- [3] S. Dresen, S. Kneisel, W. Weinmann, R. Zimmermann, and V. Auwärter, Development and validation of a liquid chromatography-tandem mass spectrometry method for the quantitation of synthetic cannabinoids of the aminoalkylindole type and methanandamide in serum and its application to forensic samples, *J. Mass Spectrom.* **46**, 163 (2011).
- [4] M. Hermanns-Clausen, S. Kneisel, B. Szabo, and V. Auwärter, Acute toxicity due to the confirmed consumption of synthetic cannabinoids: Clinical and laboratory findings, *Addiction* **108**, 534 (2013).
- [5] B. F. Cravatt, G. M. Simon, and J. R. Yates III, The biological impact of mass-spectrometry-based proteomics, *Nature (London)* **450**, 991 (2007).
- [6] S. A. Hofstadler and K. A. Sannes-Lowery, Applications of ESI-MS in drug discovery: Interrogation of noncovalent complexes, *Nat. Rev. Drug Discovery* **5**, 585 (2006).
- [7] H.-J. Kluge, High-accuracy mass spectrometry for fundamental studies, *Eur. J. Mass Spectrom.* **16**, 269 (2010).
- [8] W. C. Wiley and I. H. McLaren, Time-of-flight mass spectrometer with improved resolution, *Rev. Sci. Instrum.* **26**, 1150 (1955).
- [9] M. B. Comisarow and A. G. Marshall, Fourier transform ion cyclotron resonance spectroscopy, *Chem. Phys. Lett.* **25**, 282 (1974).
- [10] B. A. Mamyrin, V. I. Karataev, D. V. Shmikk, and V. A. Zagulin, The mass-reflectron, a new nonmagnetic time-of-flight mass spectrometer with high resolution, *Sov. Phys. JETP* **37**, 45 (1973) [*Zh. Eksp. Teor. Fiz.* **64**, 82 (1973)].
- [11] J. H. J. Dawson and M. Guilhaus, Orthogonal-acceleration time-of-flight mass spectrometer, *Rapid Commun. Mass Spectrom.* **3**, 155 (1989).
- [12] Q. Hu, R. J. Noll, H. Li, A. Makarov, M. Hardman, and R. Graham Cooks, The Orbitrap: A new mass spectrometer, *J. Mass Spectrom.* **40**, 430 (2005).
- [13] M. Yamashita and J. B. Fenn, Electrospray ion source. Another variation on the free-jet theme, *J. Phys. Chem.* **88**, 4451 (1984).
- [14] J. B. Fenn, M. Mann, C. K. Meng, S. F. Wong, and C. M. Whitehouse, Electrospray ionization for mass spectrometry of large biomolecules, *Science* **246**, 64 (1989).
- [15] M. Karas, D. Bachmann, and F. Hillenkamp, Influence of the wavelength in high-irradiance ultraviolet laser desorption mass spectrometry of organic molecules, *Anal. Chem.* **57**, 2935 (1985).
- [16] K. Tanaka, H. Waki, Y. Ido, S. Akita, Y. Yoshida, T. Yoshida, and T. Matsuo, Protein and polymer analyses up to m/z 100 000 by laser ionization time-of-flight mass spectrometry, *Rapid Commun. Mass Spectrom.* **2**, 151 (1988).
- [17] F. Hillenkamp, M. Karas, R. C. Beavis, and B. T. Chait, Matrix-assisted laser desorption/ionization mass spectrometry of biopolymers, *Anal. Chem.* **63**, 1193A (1991).
- [18] L. Schweikhard, S. Guan, and A. G. Marshall, Quadrupolar excitation and collisional cooling for axialization and high pressure trapping of ions in Fourier transform ion cyclotron resonance mass spectrometry, *Int. J. Mass Spectrom. Ion Process.* **120**, 71 (1992).
- [19] J. W. Hager, A new linear ion trap mass spectrometer, *Rapid Commun. Mass Spectrom.* **16**, 512 (2002).
- [20] I. V. Chernushevich and B. A. Thomson, Collisional cooling of large ions in electrospray mass spectrometry, *Anal. Chem.* **76**, 1754 (2004).
- [21] A. N. Krutchinsky, A. V. Loboda, V. L. Spicer, R. Dworschak, W. Ens, and K. G. Standing, Orthogonal injection of matrix-assisted laser desorption/ionization ions into a time-of-flight spectrometer through a collisional damping interface, *Rapid Commun. Mass Spectrom.* **12**, 508 (1998).
- [22] A. V. Loboda, S. Ackloo, and I. V. Chernushevich, A high-performance matrix-assisted laser desorption/ionization orthogonal time-of-flight mass spectrometer with collisional cooling, *Rapid Commun. Mass Spectrom.* **17**, 2508 (2003).
- [23] A. Makarov, E. Denisov, A. Kholomeev, W. Balschun, O. Lange, K. Strupat, and S. Horning, Performance evaluation of a hybrid linear ion trap/orbitrap mass spectrometer, *Anal. Chem.* **78**, 2113 (2006).
- [24] D. Douglas and J. French, Collisional focusing effects in radio frequency quadrupoles, *J. Am. Soc. Mass Spectrom.* **3**, 398 (1992).
- [25] D. J. Larson, J. C. Bergquist, J. J. Bollinger, W. M. Itano, and D. J. Wineland, Sympathetic cooling of trapped ions: A laser-cooled two-species nonneutral ion plasma, *Phys. Rev. Lett.* **57**, 70 (1986).
- [26] T. Baba and I. Waki, Cooling and mass-analysis of molecules using laser-cooled atoms, *Jpn. J. Appl. Phys.* **35**, L1134 (1996).
- [27] M. Bussmann, U. Schramm, D. Habs, V. Kolhinen, and J. Szerypo, Stopping highly charged ions in a laser-cooled one component plasma of ions, *Int. J. Mass Spectrom.* **251**, 179 (2006).
- [28] R. Cazan, C. Geppert, W. Nörtershäuser, and R. Sánchez, Towards sympathetic cooling of trapped ions with laser-cooled Mg^+ ions for mass spectrometry and laser spectroscopy, *Hyperfine Interact.* **196**, 177 (2010).
- [29] Z. Andelkovic, R. Cazan, W. Nörtershäuser, S. Bharadia, D. M. Segal, R. C. Thompson, R. Jöhren, J. Vollbrecht, V. Hannen, and M. Vogel, Laser cooling of externally produced Mg ions in a Penning trap for sympathetic cooling of highly charged ions, *Phys. Rev. A* **87**, 033423 (2013).
- [30] A. Ostendorf, C. B. Zhang, M. A. Wilson, D. Offenberger, B. Roth, and S. Schiller, Sympathetic cooling of complex molecular ions to millikelvin temperatures, *Phys. Rev. Lett.* **97**, 243005 (2006).
- [31] D. Offenberger, C. B. Zhang, C. Wellers, B. Roth, and S. Schiller, Translational cooling and storage of protonated proteins in an ion trap at subkelvin temperatures, *Phys. Rev. A* **78**, 061401 (2008).
- [32] S. J. Schowalter, K. Chen, W. G. Rellergert, S. T. Sullivan, and E. R. Hudson, An integrated ion trap and time-of-flight mass spectrometer for chemical and photo-reaction dynamics studies, *Rev. Sci. Instrum.* **83**, 043103 (2012).
- [33] D. J. Berkeland and M. G. Boshier, Destabilization of dark states and optical spectroscopy in Zeeman-degenerate atomic systems, *Phys. Rev. A* **65**, 033413 (2002).
- [34] C. L. Jolliffe, Mass spectrometer with radial ejection, U.S. Patent No. 5,576,540 (19 November 1996) (see <http://www.freepatentsonline.com/5576540.html>).
- [35] J. Franzen, Method and device for orthogonal ion injection into a time-of-flight mass spectrometer, U.S.

- Patent No. 5,763,878 (9 June 1998) (see <http://www.freepatentsonline.com/5763878.html>).
- [36] G. Audi and A. Wapstra, The 1993 update to the atomic mass evaluation, *Nucl. Phys. A* **595**, 409 (1995).
- [37] A. A. Sonzogni, NuDat 2.0: Nuclear structure and decay data on the internet, *AIP Conf. Proc.* **769**, 574 (2005).
- [38] T. Matthey, T. Cickovski, S. Hampton, A. Ko, Q. Ma, M. Nyerges, T. Raeder, T. Slabach, and J. A. Izaguirre, ProtoMol, an object-oriented framework for prototyping novel algorithms for molecular dynamics, *ACM Trans. Math. Softw.* **30**, 237 (2004).
- [39] C. Rosales Fernández, *DEPSOLVER v2.1* (Institute of High Performance Computing, Singapore, 2008).
- [40] S. Schiller and C. Lämmerzahl, Molecular dynamics simulation of sympathetic crystallization of molecular ions, *Phys. Rev. A* **68**, 053406 (2003).
- [41] T. Baba and I. Waki, Sympathetic cooling rate of gas-phase ions in a radio-frequency-quadrupole ion trap, *Appl. Phys. B* **74**, 375 (2002).
- [42] K. Chen, S. T. Sullivan, and E. R. Hudson, Neutral gas sympathetic cooling of an ion in a Paul trap, *Phys. Rev. Lett.* **112**, 143009 (2014).
- [43] P. Blythe, B. Roth, U. Fröhlich, H. Wenz, and S. Schiller, Production of ultracold trapped molecular hydrogen ions, *Phys. Rev. Lett.* **95**, 183002 (2005).
- [44] D. Trypogeorgos and C. J. Foot, A two-frequency ion trap confining ions with widely different charge-to-mass ratios, [arXiv:1310.6294](https://arxiv.org/abs/1310.6294).
- [45] K. Jungmann, J. Hoffnagle, R. G. DeVoe, and R. G. Brewer, Collective oscillations of stored ions, *Phys. Rev. A* **36**, 3451 (1987).
- [46] G. Birkl, S. Kassner, and H. Walther, Multiple-shell structures of laser-cooled $^{24}\text{Mg}^+$ ions in a quadrupole storage ring, *Nature (London)* **357**, 310 (1992).
- [47] C. B. Zhang, D. Offenberg, B. Roth, M. A. Wilson, and S. Schiller, Molecular-dynamics simulations of cold single-species and multispecies ion ensembles in a linear Paul trap, *Phys. Rev. A* **76**, 012719 (2007).
- [48] P. F. Staunum, K. Højbjerg, P. S. Skyt, A. K. Hansen, and M. Drewsen, Rotational laser cooling of vibrationally and translationally cold molecular ions, *Nat. Phys.* **6**, 271 (2010).
- [49] S. Kahra, G. Leschhorn, M. Kowalewski, A. Schiffrin, E. Bothschafter, W. Fuß, R. de Vivie-Riedle, R. Ernstorfer, F. Krausz, R. Kienberger, and T. Schaez, A molecular conveyor belt by controlled delivery of single molecules into ultrashort laser pulses, *Nat. Phys.* **8**, 238 (2012).
- [50] Y.-P. Chang, K. Długołęcki, J. Küpper, D. Rösch, D. Wild, and S. Willitsch, Specific chemical reactivities of spatially separated 3-aminophenol conformers with cold Ca^+ ions, *Science* **342**, 98 (2013).
- [51] M. Drewsen, A. Mortensen, R. Martinussen, P. Staunum, and J. L. Sørensen, Nondestructive identification of cold and extremely localized single molecular ions, *Phys. Rev. Lett.* **93**, 243201 (2004).
- [52] K. Chen, S. J. Schowalter, S. Kotochigova, A. Petrov, W. G. Rellergert, S. T. Sullivan, and E. R. Hudson, Molecular-ion trap-depletion spectroscopy of BaCl^+ , *Phys. Rev. A* **83**, 030501 (2011).
- [53] K.-K. Ni, H. Loh, M. Grau, K. C. Cossel, J. Ye, and E. A. Cornell, State-specific detection of trapped HfF^+ by photodissociation, [arXiv:1401.5423v1](https://arxiv.org/abs/1401.5423v1).
- [54] C. M. Seck, E. G. Hohenstein, C.-Y. Lien, P. R. Stollenwerk, and B. C. Odom, Rotational state analysis of AlH^+ by two-photon dissociation, *J. Mol. Spectrosc.* **300**, 108 (2014).
- [55] P. Puri, S. J. Schowalter, S. Kotochigova, A. Petrov, and E. R. Hudson, Action spectroscopy of SrCl^+ using an integrated ion trap time-of-flight mass spectrometer, *J. Chem. Phys.* **141**, 014309 (2014).
- [56] A. Härter and J. Hecker Denschlag, Cold atom-ion experiments in hybrid traps, *Contemp. Phys.* **55**, 33 (2014).
- [57] S. Willitsch, Ion-atom hybrid systems, [arXiv:1401.1699v1](https://arxiv.org/abs/1401.1699v1).
- [58] C. Sias and M. Köhl, Hybrid quantum systems of ions and atoms, [arXiv:1401.3188v1](https://arxiv.org/abs/1401.3188v1).
- [59] W. G. Rellergert, S. T. Sullivan, S. Kotochigova, A. Petrov, K. Chen, S. J. Schowalter, and E. R. Hudson, Measurement of a large chemical reaction rate between ultracold closed-shell ^{40}Ca atoms and open-shell $^{174}\text{Yb}^+$ ions held in a hybrid atom-ion trap, *Phys. Rev. Lett.* **107**, 243201 (2011).
- [60] S. T. Sullivan, W. G. Rellergert, S. Kotochigova, and E. R. Hudson, Role of electronic excitations in ground-state-forbidden inelastic collisions between ultracold atoms and ions, *Phys. Rev. Lett.* **109**, 223002 (2012).
- [61] S. T. Sullivan, W. G. Rellergert, S. Kotochigova, K. Chen, S. J. Schowalter, and E. R. Hudson, Trapping molecular ions formed via photo-associative ionization of ultracold atoms, *Phys. Chem. Chem. Phys.* **13**, 18859 (2011).
- [62] W. G. Rellergert, S. T. Sullivan, S. J. Schowalter, S. Kotochigova, K. Chen, and E. R. Hudson, Evidence for sympathetic vibrational cooling of translationally cold molecules, *Nature (London)* **495**, 490 (2013).